Available online at www.sciencedirect.com
ScienceDirect
Cement & Concrete Composites 29 (2007) 409–420
Cement & Concrete Composites
www.elsevier.com/locate/cemconcomp

Punching shear strength of interior concrete slab–column connections reinforced with steel fibers

Kyoung-Kyu Choi [a,*], Mahmoud M. Reda Taha [a], Hong-Gun Park [b], Arup K. Maji [a]

[a] Department of Civil Engineering, University of New Mexico, Albuquerque, NM 87131, United States
[b] Department of Architecture, Seoul National University, San 56-1, Shinlim-dong, Kwanak-gu, Seoul 151-742, Republic of Korea

Received 20 February 2006; received in revised form 13 December 2006; accepted 14 December 2006
Available online 3 January 2007

Abstract

A theoretical study was performed to investigate the punching shear strength of interior slab–column connections made of steel fiber reinforced concrete (FRC). In the steel FRC slab–column connection, the shear force applied to the critical section is resisted by both the compression zone and the tension zone at the critical section. The shear capacity of the compression zone was defined by considering the interaction between the shear and the normal stresses developed at the critical section. The shear capacity of the tension zone was defined by considering the post-cracking tensile strength of FRC. By using the shear capacity, a new strength model for the punching shear strength of steel FRC slab–column connections was developed. The proposed strength model was verified using existing test results and showed very good accuracy. For convenience in design, a simplified design equation was also developed.

Keywords: Flat plate; Punching shear; Failure mechanism; Fiber reinforced concrete; Slab–column connection

1. Introduction

The slab–column connection of a flat plate is susceptible to punching shear failure. Once punching shear failure occurs, the overall resistance of the structure against gravity load is considerably reduced, which causes the separation of the slab and column, and might even cause progressive collapse of the whole structure [1–3].

According to previous experimental studies, the addition of steel fibers to concrete effectively improves the shear strength of beams [4,5] and slab–column connections [6,7]. The ability of steel fibers to enhance shear strength of concrete is attributed to the possible transfer of tensile stresses across crack surfaces, that is known as crack-bridging, when steel fibers are incorporated [8,9]. This phenomenon permits fiber reinforced concrete (FRC) to have more ductile failure than normal concrete [9,10].

Swamy and Ali [6] and Harajli et al. [11] reported that when fibers were added in a slab–column connection, the residual strength of the slab–column connection after punching shear failure increased significantly due to the enhanced structural integrity between the slab and the column. Traditional shear reinforcing method using stirrups is inapplicable to slabs with shallow depth less than 150 mm [12]. New reinforcing technique such as using headed-studs [13] or incorporating steel fibers in the slab–column connections [14] might be good alternatives. Moreover, such alternatives have also been proven effective in seismic design because of their ability to improve energy dissipation capacity of structures [15,16].

Currently, there are various existing strength models for slab–column connections including ACI 318 [12], EC 2 [17], CEB-FIP MC 90 [18], and BS 8110 [19]. These existing models were developed for normal concrete slab–column connections, thus they might not be applicable to FRC slab–column connections. While some models for punching shear of FRC exist (for example, [11]), these models do not

* Corresponding author. Tel.: +1 505 277 7481; fax: +1 505 277 1988.
E-mail address: choikk97@naver.com (K.-K. Choi).

0958-9465/$ - see front matter © 2007 Elsevier Ltd. All rights reserved.
doi:10.1016/j.cemconcomp.2006.12.003

directly link the failure criterion of FRC to the punching shear capacity of slab–column connections.

Here, we present a theoretical approach to model the punching shear strength of interior slab–column connections using steel FRC. To evaluate the punching shear strength of the slab–column connections, material failure criteria of FRC were studied. A new strength model based on the FRC failure criteria was developed to accurately estimate the punching shear strength of steel FRC slab–column connections. The proposed strength model was verified using existing test results. For easy application of the strength model in design, a simplified design equation was developed.

2. Methods

2.1. Material strength of fiber reinforced concrete

FRC exhibits material strengths enhanced from those of normal concrete: compressive strength, f'_{cf}, tensile strength, f_{ct}, and post-cracking tensile strength, f_{pc} as shown in Fig. 1. According to Narayanan and Darwish [5] and Khuntia et al. [20], the post-cracking tensile strength, f_{pc}, has the most significant effect on the structural performance of FRC.

Naaman and Reinhardt [21] showed that the strength of FRC is significantly affected by the fiber volume ratio, V_f, aspect ratio, L/D, and shape. Through probabilistic analysis based on the experimental investigations of FRC [21,22], the compressive strength, f'_{cf}, tensile strength, f_{ct}, and post-cracking tensile strength, f_{pc} of FRC were defined as

$$f'_{cf} = 1.9V_f(L/D)\beta + f'_c \quad \text{(MPa)} \tag{1a}$$

$$f_{ct} = f_t(1 - V_f) + \alpha_1\alpha_2\tau V_f(L/D) \tag{1b}$$

$$f_{pc} = \lambda_1\lambda_2\lambda_3 V_f(L/D)\tau\beta \tag{1c}$$

where f'_c is the compressive strength of an equivalent normal concrete without fibers, f_t = tensile strength of concrete under pure tension evaluated as $f_t = 0.292\sqrt{f'_c}$ (MPa), following the work of Oluokun [23] and Reda Taha et al. [24]. L = length of fiber; D = diameter of fiber; α_1 = coefficient representing the fraction of bond mobilized at first matrix cracking; α_2 = efficiency factor of fiber orientation in the uncracked state of the composite; τ = average interfacial bond strength of fiber matrix; λ_1 = expected pull-out length ratio; λ_2 = efficiency factor of orientation in the cracked state; and λ_3 = group reduction factor associated with the number of fiber pulling-out per unit area. The coefficients α_1 ($\approx$0.5) and α_2 ($\approx$0.1) were reported to be considerably small numerical values, thus it can be assumed that $f_{ct} = f_t$. Also the coefficients $\lambda_1 = 0.25$, $\lambda_2 = 1.2$, and λ_3=1.0 can be used [25]. β accounts for the effect of fiber shape and concrete type after Khuntia et al. [20] such that $\beta = 1$ for hooked or crimped steel fibers; $\beta = 2/3$ for plain or round steel fibers with normal concrete; and $\beta = 3/4$ for hooked or crimped steel fibers with lightweight concrete. Moreover, interfacial bond strength, τ, between steel fibers and concrete is an important parameter determining the post-cracking behavior of FRC [10,24]. The interfacial bond strength is strongly affected by the quality of concrete and fiber geometry and shape [24,25]. We therefore relate the bond strength of FRC to the tensile strength of the concrete such as $\tau = 2f_t$ [25]. Finally, the compressive stress–strain constitutive relationship of FRC was assumed to follow a simple parabola such that

$$\sigma_c(\varepsilon) = f'_{cf}\left[2\left(\frac{\varepsilon}{\varepsilon_{cof}}\right) - \left(\frac{\varepsilon}{\varepsilon_{cof}}\right)^2\right] \tag{2}$$

where ε_{cof} is the compressive strain corresponding to the compressive strength of FRC taken equal to $0.00079 \cdot V_f(L/D) + 0.0041(f'_{cf}/f'_c)$ following the work of Fanella and Naaman [22], ε is the strain at any point in the cross-section, and $\sigma_c(\varepsilon)$ is the compressive strain at this point.

2.2. Failure criteria of fiber reinforced concrete

Generally, since a flat plate has a large span-to-thickness ratio, its behavior is dominated by flexural deformation. Flexural cracking and yielding of reinforcing bars that occur prior to punching shear failure have been observed experimentally [26,27]. The maximum observed flexural crack width at slab–column connections was about 4 mm [27]. Such crack width would significantly downplay shear contributions due to aggregate interlock and dowel actions [26,28,29]. Shear strength in flexure-dominated members

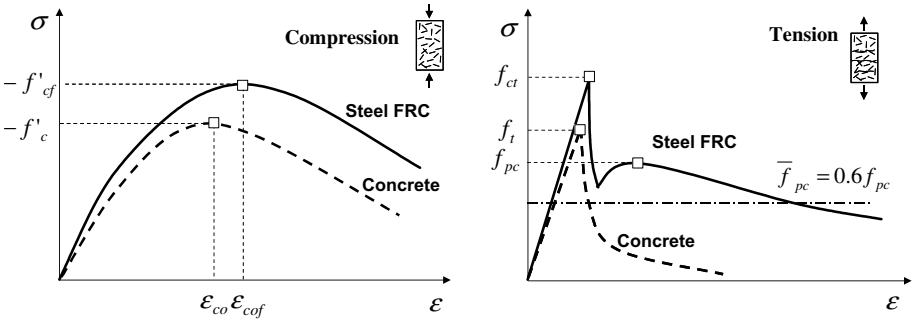

Fig. 1. Stress–strain relationship of FRC.

was attributed to the compression zone of intact concrete which prevented shear-slip of the crack surfaces [26,30].

Based on the results, we assume that shear resistance of the FRC slab–column connections is provided mainly by the contribution of the intact concrete in the compression zone. This assumption is supported with many observations of other studies on normal concrete slab–column connections [31–33]. However, the major difference in FRC slab–column connections, is that after cracking occurs, tensile stress is transferred across the crack surfaces by the fibers. Therefore, unlike conventional concrete slab–column connections, the tension zone of FRC slab–column connections contributes to the shear resistance by means of the post-cracking tensile strength. Therefore, the overall shear strength of FRC slab–column connections is defined as the sum of contributions of the compression and the tension zones.

Fig. 2 shows the governing stress components developing in the compression zone of the critical section at the slab–column connection. The compression zone of the critical section is subjected to combined normal and shear stresses. Therefore, the interaction between these stress components must be considered to accurately evaluate the punching shear strength of the slab–column connection [32]. Fig. 2 shows the development of three-dimensional stresses at the critical section: two orthogonal normal stresses (σ_{c1} and σ_{c2}) and shear stresses (v_{c1} and v_{c2}). The normal stress (σ_{c2}) and shear stress (v_{c2}) acting on the face orthogonal to the cross-section might affect the punching shear strength of the slab–column connection. However, because of the high rigidity of the slab–column joint, these stresses are directly transmitted to the column through the corner of the column section [34]. Thus, the three-dimensional stresses that develop at the critical section can be simplified as two-dimensional compressive and shear stresses, σ_c (=σ_{c1}) and v_c (=v_{c1}), acting on the cross-section of the compression zone, following the work of the Eurocode 2 [17] and the CEB-FIP [18].

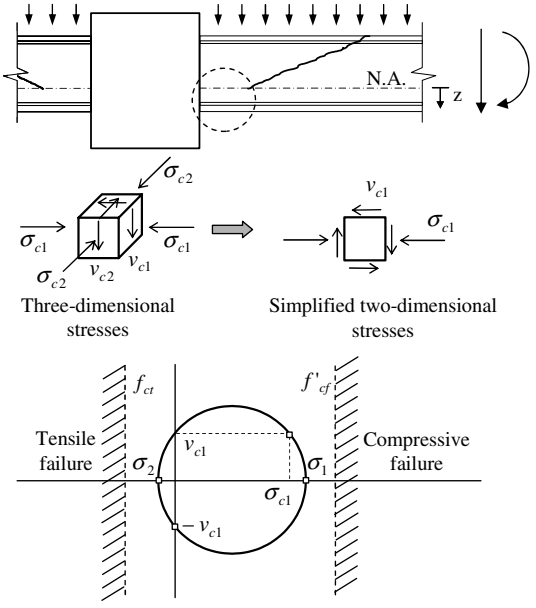

Fig. 2. Rankine's failure criteria of fiber reinforced concrete.

Considering the normal and shear stress states at the cross-section, the constitutive material failure mechanism can be defined using Rankine's failure criterion [35]. In this failure criterion, material failure occurs when the principal stress resulting from the combined stresses reaches the material strength. When the principal compressive stress reaches the compressive strength of FRC – f'_{cf}, a failure controlled by compression occurs, and when the principal tensile stress reaches the tensile strength f_{ct} (=f_t), a failure controlled by tension occurs. The failure criteria of the compression zone thus can be defined as

$$\sigma_1 = -\frac{\sigma_c}{2} - \sqrt{\left(\frac{\sigma_c}{2}\right)^2 + v_c^2} = -f'_{cf}$$

for failure controlled by compression (3a)

$$\sigma_2 = -\frac{\sigma_c}{2} + \sqrt{\left(\frac{\sigma_c}{2}\right)^2 + v_c^2} = f_{ct}$$

for failure controlled by tension (3b)

σ_1 and σ_2 = principal compressive and tensile stresses, respectively. σ_c ($\geqslant 0$) and v_c = compressive normal stress and shear stress of FRC, respectively.

As the contribution of FRC to punching shear strength is taken into account, the effect of the multi-axial state of stress on the tensile strength of FRC shall also be considered [36]. In the present study, it was assumed that FRC follows a similar trend to that of conventional concrete; In tension–compression, the tensile strength of concrete, f_t, is reduced by the transverse compressive stress, σ_1 (Fig. 3). Thus the reduced tensile strength of FRC f'_{ct}, was considered as

$$\left(\frac{f'_{ct}}{f_{ct}}\right) = \left(\frac{f'_t}{f_t}\right) = \left[1 - 0.5\left(\frac{f_t}{f'_c}\right)\left(\frac{\sigma_1}{\sigma_2}\right)\right]^{-1} \leqslant 1 \quad (4)$$

where $\sigma_1 \leqslant 0$ and $\sigma_2 > 0$.

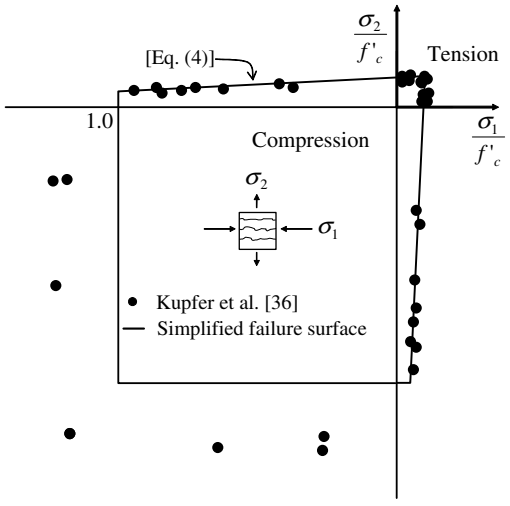

Fig. 3. Plane stress failure criteria of concrete.

From Eq. (2), the maximum shear stress can be defined as a function of the normal stress. Since the compressive stress in the compression zone, σ_c, varies with the distance from the neutral axis, the maximum shear stress at each location in the compression zone is defined as a function of the distance from the neutral axis z as

$$v_c(z) = \sqrt{f'_{cf}[f'_{cf} - \sigma_c(z)]}$$

for failure controlled by compression (5a)

$$v_c(z) = \sqrt{f'_{ct}[f'_{ct} + \sigma_c(z)]}$$

for failure controlled by tension (5b)

At a cross-section of a flexure-dominated member, the distribution of compressive normal stress is affected by the curvature (Fig. 4a and b) of the cross-section as well as the amount of flexural reinforcement. Fig. 4c shows the variations of the compressive normal stress, and Fig. 4d and e shows the variations of the maximum shear stress according to the curvature of the cross-section. In these figures, $\alpha\varepsilon_{cof}$ = compressive strain at the extreme compression fiber of a cross-section, and ε_{cof} = compressive strain corresponding to the compressive strength of FRC. Fig. 5 presents closely the variation of maximum shear stress controlled by tension.

As the curvature of the cross-section (representing the degree of flexural damage) increases, the depth of the compression zone decreases, and the distribution of compressive stress and maximum shear stress varies. Before flexural cracking occurs in the tension zone (Stage AB in Fig. 4), the shear force is resisted by the entire cross-section and the neutral axis is approximately located at the centroid of the cross-section. After the flexural cracking (Stage BC), the tensile crack propagates to the neutral axis and the shear resistance developed by the tension zone significantly decreases. After the tensile crack reaches the neutral axis (Stage CE), the compression zone of intact concrete mainly develops the shear resistance, and the magnitude and distribution of the maximum shear stress at the compression zone is affected by the compressive normal stress (Figs. 4c, d and e and 5, and Eqs. (5a) and (5b)). After the compressive normal stress at the extreme compression fiber of the cross-section reaches the compressive strength of concrete ($\alpha\varepsilon_{cof} > \varepsilon_{cof}$), it is assumed that the part of the compression zone experiencing compressive damage no longer develops shear resistance (Fig. 5). Therefore, the shear capacity of the cross-section is provided only by the remaining part of the compression zone that did not experience compression softening ($0 \leqslant z \leqslant c_u/\alpha$). As a result, the shear capacity of the cross-section decreases as the deformation of the cross-section increases.

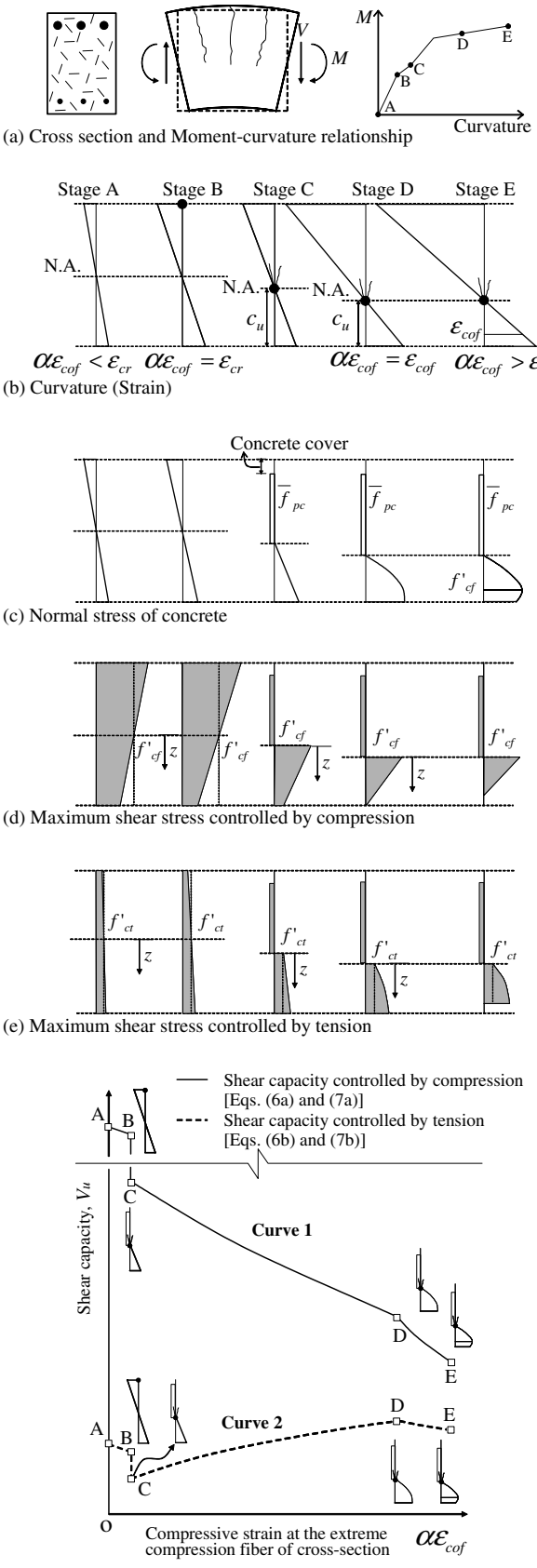

Fig. 4. Variations of normal stress and corresponding shear capacity according to curvature at slab–column connection.

2.3. Punching shear capacity at a cross-section

At the potential critical section of a slab–column connection, a failure controlled by compression or tension

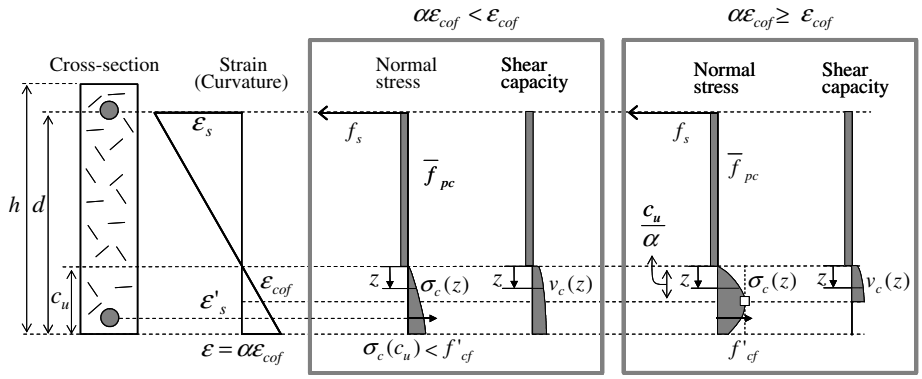

Fig. 5. Profile of maximum shear stress controlled by tension.

can occur. The shear capacity at the potential critical section can be calculated by integrating the maximum shear stresses (Eq. (5)). Fig. 4f shows schematically the variations of the shear capacity according to flexural deformation (curvature). Curves 1 and 2 indicate the shear capacities controlled by compression and tension, respectively. The shear capacity in Stage AB is developed by the entire cross-section. Therefore,

For failure controlled by compression

$$V_u = \int_{-h/2}^{h/2} b(z)v_c(z)\,dz = \int_{-h/2}^{h/2} b(z)\sqrt{f'_{cf}[f'_{cf} - \sigma_c(z)]}\,dz \quad (6a)$$

For failure controlled by tension

$$V_u = \int_{-h/2}^{h/2} b(z)v_c(z)\,dz = \int_{-h/2}^{h/2} b(z)\sqrt{f'_{ct}[f'_{ct} + \sigma_c(z)]}\,dz \quad (6b)$$

where $b(z)$ = perimeter of the critical section, and h = depth of slab. After tensile cracking is initiated (Stage BC), the shear capacity decreases because the allowable maximum shear stress in the tension zone significantly decreases as a result of cracking. After the tensile cracking reaches the neutral axis (Stage CD), the shear capacity controlled by tension increases because the compressive normal stress that is increasing with flexural deformation (or $\alpha\varepsilon_{cof}$) prevents the propagation of the diagonal tension cracks in the compression zone. On the other hand, in Stage CD, the shear capacity controlled by compression is continuously decreased as a result of the increasing compressive normal stress. In Stage CD, the tension zone can develop shear resistance even after tensile cracking due to post-cracking tensile strength of FRC. Therefore, the shear capacity of the cross-section is defined as the sum of the contributions of the compression zone and the tension zone.

For failure controlled by compression

$$V_u = V_c + V_{fr} = \int_0^{c_u} b(z)\sqrt{f'_{cf}[f'_{cf} - \sigma_c(z)]}\,dz + V_{fr} \quad (7a)$$

For failure controlled by tension

$$V_u = V_c + V_{fr} = \int_0^{c_u} b(z)\sqrt{f'_{ct}[f'_{ct} + \sigma_c(z)]}\,dz + V_{fr} \quad (7b)$$

where V_c = contribution of compression zone to shear capacity after tensile cracking, and V_{fr} = contribution of the tension zone to shear capacity after tensile cracking, and c_u = depth of the compression zone. In an actual beam with inclined tensile cracks, V_{fr} is affected by the direction of the inclined tensile cracks, $\bar{\phi}$ as well as the post-cracking tensile strength of FRC, f_{pc}.

Numerical studies for the above Eqs. (7a) and (7b) showed that generally, the shear capacity controlled by compression is greater than the shear capacity controlled by tension. An exemplar case is shown in Fig. 6 for a 500 width × 200 thickness (mm) cross-section in a normal concrete slab–column connection ($V_{fr} = 0$). Such results indicate that the shear capacity of the compression zone

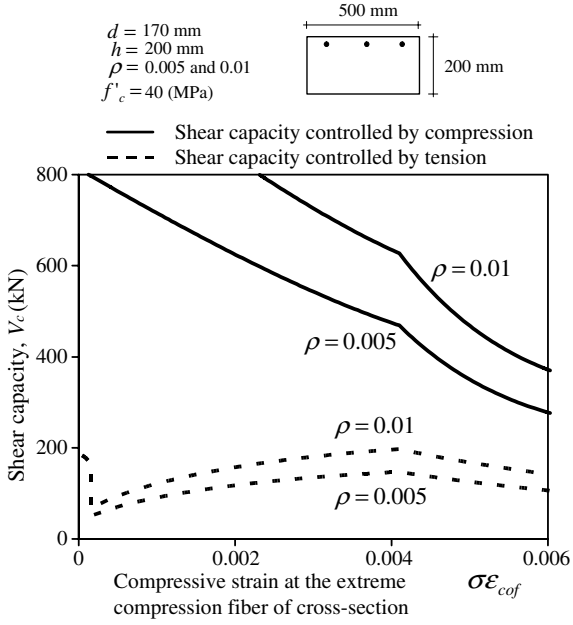

Fig. 6. Components of shear capacities controlled by compression and tension for slab models.

is generally governed by tension failure rather than by compression failure. This conclusion is supported by findings of other researchers [26]. The shear capacity of FRC slab–column connections is expected to show a similar trend to that of the normal concrete connections, though the shear capacity of FRC slab–column connections is increased due to the post-cracking strength of FRC. Thus, in the present study, the shear capacity controlled by tension was considered to predict the shear strength of FRC slab–column connections.

To evaluate the punching shear capacity at the critical section, it was assumed that along the depth of the compression zone, the strain of concrete was linearly distributed. Considering the stress–strain constitutive relationship of FRC (Eq. (2)), the stress at any point in the cross-section with tensile cracks can be evaluated as

$$\sigma_c(z) = f'_{cf}\left[2\left(\frac{\alpha z}{c_u}\right) - \left(\frac{\alpha z}{c_u}\right)^2\right] \tag{8}$$

For simplicity in calculation, we considered the average compressive stress $\bar{\sigma}$ over the compression zone. Thus, the shear capacity of the cross-section controlled by tension is redefined as

$$V_u \approx \sqrt{f'_{ct}[f'_{ct} + \bar{\sigma}]}\, b_0 c_u + V_{fr} \quad \text{for } f_{ct}/E_c < \alpha\varepsilon_{cof} < \varepsilon_{cof} \tag{9a}$$

$$V_u \approx \sqrt{f'_{ct}[f'_{ct} + \bar{\sigma}]}\, b_0 c_u/\alpha + V_{fr} \quad \text{for } \alpha\varepsilon_{cof} \geqslant \varepsilon_{cof} \tag{9b}$$

where

$$\bar{\sigma} = \frac{\int_0^{c_u} \sigma_c(z)\,dz}{c_u} = \left(\alpha - \frac{\alpha^2}{3}\right) f'_{cf} \tag{10}$$

b_0 = average perimeter of the critical section in the compression zone of a slab–column connection.

3. Punching shear strength

Fig. 7 shows the relationship between the shear capacity curve and the shear demand curve at a potential critical section of a slab–column connection. The shear capacity curve represents the shear capacity varying with the flexural deformation (or compressive strain at the extreme compression fiber of the cross-section) (Eqs. (6b) and (7b) or (9a) and (9b)). The shear demand curve represents the shear force which is applied to the critical section by the flexural deformation of the slab. As shown in Fig. 7, the punching shear strength of the critical section can be determined at the intersection between the shear capacity curve and the shear demand curve. In an actual slab, since the shear capacity and shear demand vary according to the location of each potential critical section, punching shear failure must be examined at all possible critical sections at the slab–column connection. The first possible critical section, where the shear demand reaches the shear capacity, becomes the critical section. The punching shear strength of the slab–column connection is determined as the shear capacity of the critical section.

According to previous test results, punching shear failure usually occurs near the slab–column connection. This is because at the slab–column connection, the flexural cracking is most severe and the perimeter of the critical section reaches its minimum, and thus the punching shear capacity is significantly reduced (Eq. (9)). On the other hand, the punching shear demand reaches its maximum at the slab–column connection. Therefore, in the present study, the critical section was defined as the cross-section with the minimum possible perimeter, which is close to the slab–column connection.

Fig. 8 shows the truncated pyramid-shaped failure surface of a slab–column connection. The failure surface inclined with angle $\bar{\phi}$ is composed of the failure surface of the tension zone and that of the compression zone. In the present study, for simplicity, the critical section for the compression zone was defined approximately, as a rectangular cross-section, by using the average perimeter b_0 of the truncated pyramid-shaped failure surface in the compression zone. The cross-sectional area of the inclined tension zone A_T and that of the compression zone A_C can be calculated by using the average punching shear cracking angle $\bar{\phi}$ as (Fig. 8)

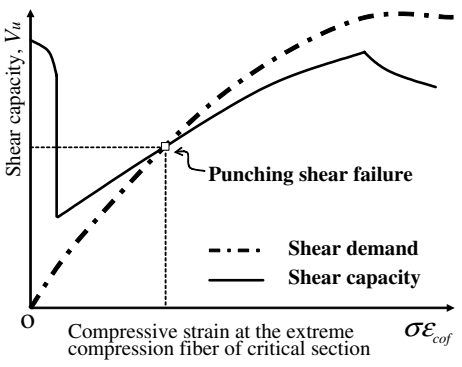

Fig. 7. Determination of punching shear strength.

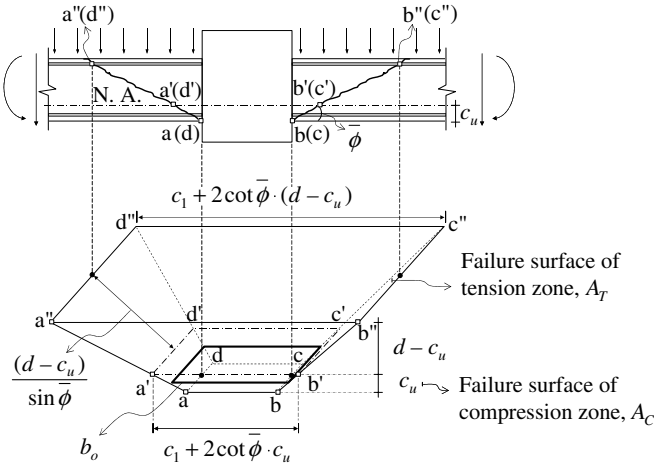

Fig. 8. Critical section of punching shear for proposed model.

$$A_T = (2c_1 + 2c_2 + 4\cot\bar{\phi}\cdot d)(d - c_u)/\sin\bar{\phi} \quad (11)$$

$$A_C = b_0 c_u = (2c_1 + 2c_2 + 4\cot\bar{\phi}\cdot c_u)c_u \quad (12)$$

Considering the shear capacity in the tension zone to be provided by only post-cracking tensile strength $\bar{f}_{pc}$, an average post-cracking tensile strength, $\bar{f}_{pc} = 0.6f'_{pc}$, can be used following the work of Naaman and Reinhardt [37]. The shear strength provided by the tension zone V_{fr} is defined as Eq. (13) with $\bar{f}_{pc}$ (Fig. 9).

$$V_{fr} = \bar{f}_{pc} A_T \cos\bar{\phi} \quad (13)$$

Based on experimental observations showing FRC slab–column connection to have a relatively lower punching shear crack angle compared to normal concrete slab–column connection, the average cracking angle $\bar{\phi}$ was set to 30°. We will show that an assumption of this cracking angle $\bar{\phi} = 30^\circ$ can be used without deteriorating model accuracy. The proposed shear capacity curve in Eq. (9) was applied to specimen FS-2 tested by Theodorakopoulos and Swamy [7] (Fig. 10). The result is shown in Fig. 11.

To determine the shear strength of the slab–column connection, the shear demand curve was evaluated by using the effective beam model [38]. Assuming the flat plate as two orthogonal beams with effective widths, $\gamma l_1 = 2c_1 + (1/3)l_2$, and $\gamma l_2 = 2c_2 + (1/3)l_1$ [38], the moments at the critical section, M_{u1} and M_{u2}, can be estimated for a given value of curvature ψ (or compressive strain at extreme compression fiber $\alpha\varepsilon_{cof}$) (Fig. 12). Then the shear force (shear demand) acting on the critical section V_d, which is developed by M_{u1} and M_{u2}, can be calculated as

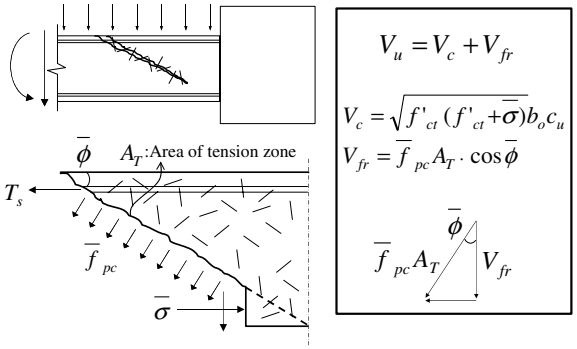

Fig. 9. Shear resistance at FRC slab–column connection.

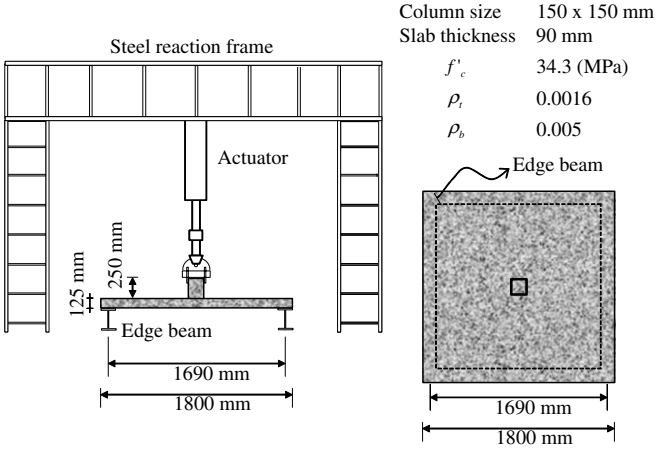

Fig. 10. Test setup for Theodorakopoulos and Swamy's [7] specimen FS-2.

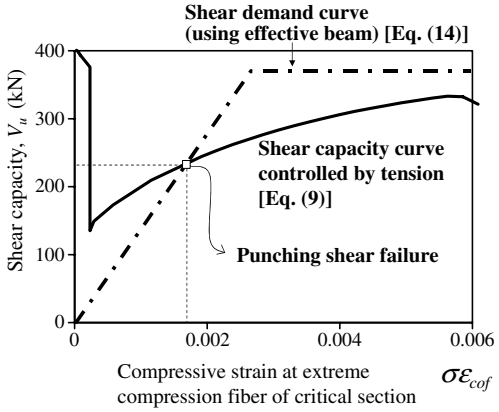

Fig. 11. Determination of punching shear strength of Theodorakopoulos and Swamy's [7] FS-2.

$$V_d = 2V_{d1} + 2V_{d2} \quad (14)$$

$$V_{d1} = \frac{M_{u1}}{l_2/2 - c_2/2 - \cot\bar{\phi}\cdot c_u/2} \leqslant V_{d1y} \quad (15a)$$

$$V_{d2} = \frac{M_{u2}}{l_1/2 - c_1/2 - \cot\bar{\phi}\cdot c_u/2} \leqslant V_{d2y} \quad (15b)$$

where

$$V_{d1y} = \frac{[\rho_{t1} d f_y + \bar{f}_{pc}(d - c_u)](\gamma l_2)(jd)}{l_2/2 - c_2/2 - \cot\bar{\phi}\cdot c_u/2} \quad (16a)$$

$$V_{d2y} = \frac{[\rho_{t2} d f_y + \bar{f}_{pc}(d - c_u)](\gamma l_1)(jd)}{l_1/2 - c_1/2 - \cot\bar{\phi}\cdot c_u/2} \quad (16b)$$

l_1 and l_2 = span length in longitudinal and transverse directions, respectively, ρ_{t1} and ρ_{t2} = ratios of flexural reinforcement of the effective beams in longitudinal and transverse directions, respectively, M_{u1} and M_{u2} = moments corresponding to curvature (or compressive strain at extreme compression fiber) at the critical sections of the effective beams, V_{d1y} and V_{d2y} = shear force provided by the flexural strength of the effective beams in longitudinal and transverse directions, respectively, and jd = length of moment arm of the effective beams. Fig. 11 shows the shear demand curve (Eq. (14)) for specimen FS-2 of Theodorakopoulos and Swamy [7]. At the intersection between the shear capacity curve and the shear demand curve, the shear strength of the specimens was 240 kN, which agreed well with the test result $V_{exp} = 225$ kN.

4. A simplified approach and verification

Since the evaluation of the shear capacity curve and the shear demand curve requires considerable calculation, a simplified approach for evaluating the shear strength of

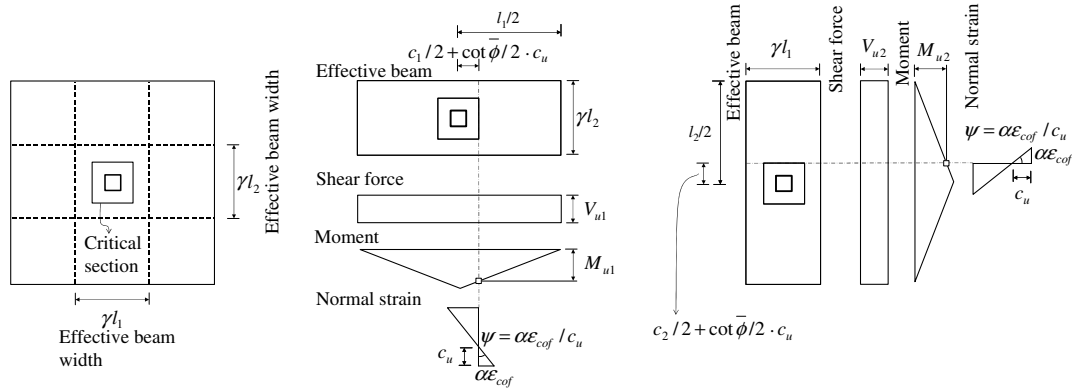

(a) Idealized effective beams (b) Longitudinal direction (c) Transverse direction

Fig. 12. Effective beam model for flat plate simply supported on four edges.

FRC slab–column connections is proposed here considering the above findings and observations by several researchers. If a design value of the maximum compressive strain corresponding to the punching shear failure is assumed, the punching shear strength of a slab–column connection can be easily calculated without evaluating the shear capacity curve and the shear demand curve. Based on the test results on conventional concrete slab–column connections performed by Kinnunen and Nylander [31], the maximum compressive strain corresponding to the punching shear failure, $\alpha\varepsilon_{cof} = 0.00196$, can be used. For such maximum compressive strain, the average compressive stress $\bar{\sigma}$ can be calculated using Eq. (10). This will further simplify the tensile strength of FRC to $f'_{ct} = 0.9f_t$ (Eq. (4)). Using Eq. (9a), the punching shear strength of FRC slab–column connections can be defined as

$$V_u = \sqrt{0.9f_t[0.9f_t + (\alpha - \alpha^2/3)\cdot f'_{cf}]}A_C + V_{fr} \quad (17)$$

Finally, to address the size effect of punching shear strength reported by a few researchers [39,40], a size effect factor λ_s [$= \sqrt[4]{400/d}$ (mm)] specified in BS 8110 [19] was used. Using λ_s, the punching shear strength of the FRC slab–column connection can be redefined as

$$V_n = \lambda_s\sqrt{0.9f_t[0.9f_t + (\alpha - \alpha^2/3)\cdot f'_{cf}]}A_C + V_{fr} \quad (18)$$

where $\lambda_s = \sqrt[4]{400/d}$, d in mm.

For verification, the proposed strength model (Eq. (18)) was applied to specimens presented in Table 1. In the comparison, 53 steel FRC specimens tested by five researchers [6,7,11,41,42] were used. All of these specimens were simply supported flat plates with testing setup similar to that in Fig. 10. The dimensions and properties of the specimens were summarized in Table 1. In this comparison, the specimens with only steel FRC were used, and those with other type of fibers and those with shear reinforcement were not included. Various shapes of steel fibers were used: crimped, hooked, Japanese type, paddle, corrugated, and plain fibers. Various shapes of the cross-sections of fibers were used: circular, rectangular, and elliptical cross-sections. For a fiber with a non-circular cross-section, the aspect ratio of fiber (L/D) was calculated by using the diameter of an equivalent circular cross-section which has the same area as that of the original cross-section of the fiber. The test specimens had a broad range of design parameters which enables good verification of the proposed model: $12.5 \leqslant f'_c \leqslant 41.2$ (MPa), $1.0 \leqslant c_1/d \leqslant 2.6$, $11.8 \leqslant l_1/d \leqslant 20.1$, $39 \leqslant d \leqslant 138$ (mm), $0.33 \leqslant \rho \leqslant 2.03$ (%), $0 \leqslant V_f \leqslant 2.8$ (%), $29 \leqslant L/D \leqslant 100$. For all calculations, the cracking angle was taken equal to 30° as discussed above.

In Fig. 13, the punching shear strength predicted by the proposed strength model (Eq. (18)) is compared with the test results. It is obvious that the proposed strength model can accurately predict the punching shear strength of the test specimens. The mean value of the experimental results to the model prediction is 1.00, with a standard deviation of 11.7%. These results showed that the proposed model can predict the punching shear strength of specimens with various types of steel fibers including plain, hooked, and crimped fibers with good accuracy (Fig. 14).

Fig. 15 shows the variation of the punching shear strengths of slab–column connections according to primary design parameters: the compressive strength of concrete, flexural reinforcement ratio, and the volume ratio of fiber. As shown in Fig. 15a, the punching shear strength increases with the compressive strength of concrete. This is because the tensile strength of FRC increases as the compressive strength of FRC increases. In Fig. 15b, as flexural reinforcement ratio increases, the punching shear strength increases. In the proposed strength model (Eq. (18)), the punching shear strength of a slab–column connection is affected by the depth of the compression zone c_u. As the flexural reinforcement ratio increases, the depth of the compression zone c_u increases, which results in the increase of the punching shear strength. As shown in Fig. 15c, the proposed strength model accurately predicts the punching shear strength, which varies according to the volume ratio of fibers. The results are compared to the existing ACI model for the punching shear strength of normal concrete slab–column connections [12] which does not acknowledge

Table 1
Dimensions and properties of test specimens, and strength-predictions

Specimens		V_f (%)	L/D[a]	Fiber type	d (mm)	c_1, c_2 (mm)	f'^c_c (MPa)	Tensile reinforcement ratio, ρ (%)	$V_{exp.}$ (kN)	$\frac{V_{exp.}}{V_{pred.}}$[d]
Swamy and Ali [6]	S-1	0	–	–	105	150	34.3	0.50	198	1.10
	S-2	0.6	100	Crimped	105	150	34.3	0.50	244	1.03
	S-3	0.9	100	Crimped	105	150	34.3	0.50	263	1.01
	S-4	1.2	100	Crimped	105	150	34.3	0.50	281	0.98
	S-5	0.9	100	Crimped	105	150	34.3	0.50	267	1.02
	S-6	0.9	100	Crimped	105	150	34.3	0.50	239	0.91
	S-7	0	–	–	105	150	34.3	0.66	222	1.10
	S-13	0.9	83	Plain	105	150	34.3	0.66	237	0.98
	S-12	0.9	100	Hooked	105	150	34.3	0.66	249	0.90
	S-11	0.9	100	Crimped	105	150	34.3	0.66	262	0.95
	S-8	0.9	100	Crimped	105	150	34.3	0.66	256	0.91
	S-16	0.9	100	Crimped	105	150	34.3	0.50	213	0.81
	S-10	0.9	100	Crimped	105	150	34.3	0.42	203	0.81
	S-9	0.9	100	Crimped	105	150	34.3	0.33	179	0.75
	S-19	0	–	–	105	150	34.3	0.33	131	0.88
Theodorakopoulos and Swamy [7]	FS-1	0	–	–	100	150	31.1	0.56	174	1.00
	FS-2	0.5	100	Crimped	100	150	29.9	0.56	225	1.08
	FS-3	1	100	Crimped	100	150	31.4	0.56	247	1.00
	FS-4	1	100	Crimped	100	150	32.9	0.56	224	0.87
	FS-5	1	100	Crimped	100	150	33.5	0.37	198	0.84
	FS-6	1	100	Crimped	100	150	31.4	0.37	175	0.75
	FS-7	1	100	Crimped	100	150	32.3	0.37	192	0.83
	FS-19	0	–	–	100	150	30.4	0.37	137	0.95
	FS-20	1	100	Crimped	100	150	32.6	0.37	211	0.90
	FS-8	0	–	–	100	100	32.3	0.56	150	1.00
	FS-9	1	100	Crimped	100	100	31.3	0.56	217	1.02
	FS-10	0	–	–	100	200	32.0	0.56	191	0.97
	FS-11	1	100	Crimped	100	200	30.1	0.56	260	0.94
	FS-12	1	60	Japanese[b]	100	150	31.8	0.56	218	0.98
	FS-13	1	100	Hooked	100	150	29.5	0.56	236	0.98
	FS-14	1	70	Crimped	100	150	30.8	0.56	240	1.06
	FS-15	1	90	Paddle[b]	100	150	27.5	0.56	238	1.05
	FS-16	1	70	Paddle[b]	100	150	24.6	0.56	228	1.12
	FS-17	1	70	Paddle[b]	100	150	41.2	0.56	268	1.05
	FS-18	1	70	Paddle[b]	100	150	12.5	0.56	166	1.13
Harajli et al. [11]	A1	0	–	–	39	100	29.6	1.12	63	1.11
	A2	0.45	100	Hooked	39	100	30.0	1.12	68	1.10
	A3	0.8	100	Hooked	39	100	31.4	1.12	78	1.17
	A4	1	60	Hooked	39	100	24.6	1.12	69	1.18
	A5	2	60	Hooked	39	100	20.0	1.12	62	1.12
	B1	0	–	–	55	100	31.4	1.12	99	1.09
	B2	0.45	100	Hooked	55	100	31.4	1.12	115	1.14
	B3	0.8	100	Hooked	55	100	31.8	1.12	117	1.10
	B4	1	60	Hooked	55	100	29.1	1.12	118	1.18
	B5	2	60	Hooked	55	100	29.2	1.12	146	1.34
Alexander and Simmonds [41]	P11F0	0	–	–	138	200	33.2	0.43	257	0.99
	P11F3	1.3	29	Corrugated[b]	138	200	35.8	0.43	324	0.98
	P11F66	2.7	29	Corrugated[b]	138	200	35.0	0.43	345	0.87
	P38F0	0	–	–	111	200	36.9	0.54	264	1.08
	P38F34	1.4	29	Corrugated[b]	111	200	38.4	0.54	308	1.04
	P38F69	2.8	29	Corrugated[b]	111	200	38.5	0.54	330	0.96
McHarg et al. [42]	FSU	0.5	60	Hooked	117	225	39.0	1.04	422	1.12
	FSB	0.5	60	Hooked	117	225	39.0	2.03	438	0.93
Mean										1.00
Standard deviation										0.117

[a] Aspect ratios of fibers calculated with diameters of equivalent circular cross-sections.
[b] $\beta = 1$ was used.
[c] Some of these data were calculated by using $f'_c = f_{c,\,cube}/1.42$, $f_{c,cube}$ = compressive cube strength of concrete.
[d] Strength-predictions by proposed method, Eq. (18).

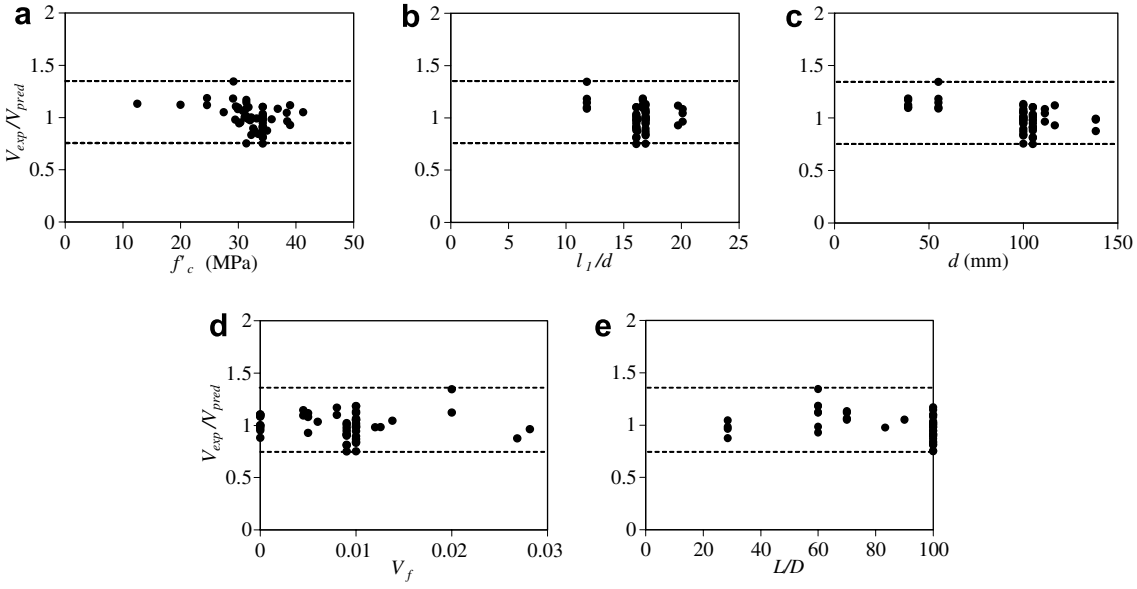

Fig. 13. Strength-predictions for test specimens by proposed model.

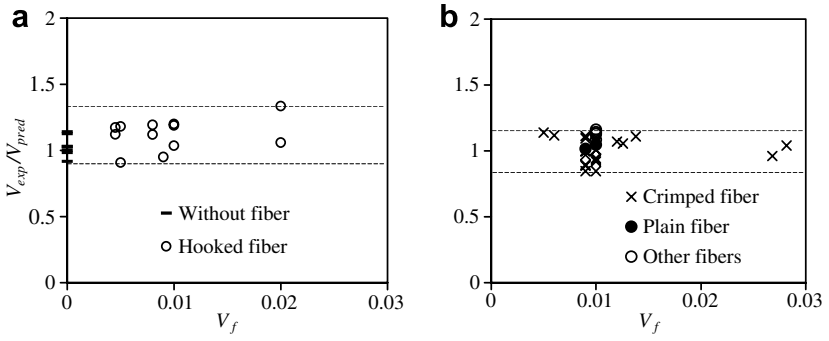

Fig. 14. Strength-predictions for test specimens using various types of steel fibers.

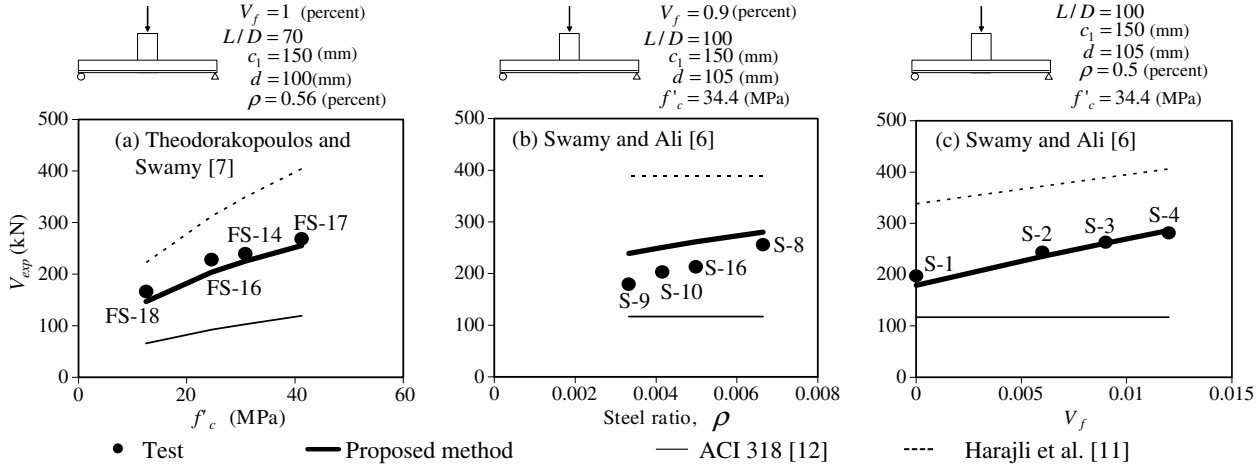

Fig. 15. Variations of punching shear strength according to design parameters.

post-cracking capacity of FRC. It is obvious that the proposed method can predict the punching shear strength of FRC with much better accuracy than the ACI model. The ACI model [12] underestimates the punching shear capacity of FRC due to its neglect of the post-cracking capacity which can significantly contribute to the punching shear strength capacity of the slab–column connections reinforced with steel fibers.

It is noted that the proposed strength model with proper modification developed in the present study may be applicable to the other types of connections subjected to unbalanced moment. However, since experimental studies on edge or corner connections using steel fibers were rarely performed, it is difficult to verify the model applicability to edge and corner connections. Therefore, the scope of the present study was limited to interior slab–column connections.

5. Conclusions

A theoretical model for evaluating the punching shear strength of slab–column connections reinforced with steel fibers was developed. The contributions of the compression zone and the tension zone at the critical section were considered. The contribution of the compression zone was evaluated by considering the variation of the compressive stress developed by the flexural moment. The contribution of the tension zone was evaluated by considering the effect of the post-cracking tensile strength which is an important characteristic of FRC. A simplified strength model for design purpose was developed. The proposed strength model was verified by the comparisons with the existing test results of slab–column connections reinforced with steel fibers. The punching shear capacity of the compression zone as well as that of the tension zone was controlled by tension cracking rather than compression crushing. The shear capacities of the compression zone and the tension zone were strongly affected by the depth of the compression zone and the post-cracking tensile strength of FRC, respectively. The use of FRC significantly enhanced the punching shear capacity of slab–column connections.

Acknowledgements

The financial support by the Defense Threat Reduction Agency (DTRA)-University of New Mexico Strategic Partnership and the Ministry of Construction and Transportation of Korea (04R&D C02-02) is greatly appreciated.

References

[1] Feld J. Lessons from failures of concrete structures. ACI monograph, vol. 1. Detroit: American Concrete Institute/Iowa State University Press; 1964. p. 30–2.
[2] Building collapse blamed on design, construction. Eng News-Rec 1971;187:19.
[3] Collapse kills five and destroys large portion of 26-story building under way. Eng News-Rec 1973;190(10):12.
[4] Mansur MA, Ong KCG, Paramsivam P. Shear strength of fibrous concrete beams without stirrups. J Struct Eng 1986;112(9):2066–79.
[5] Narayanan R, Darwish IYS. Use of steel fibers as shear reinforcement. ACI Struct J 1987;84(3):216–27.
[6] Swamy RN, Ali SAR. Punching shear behavior of reinforced slab–column connections made with steel fiber concrete. ACI J 1982;79(6):392–406.
[7] Theodorakopoulos DD, Swamy N. Contribution of steel fibers to the strength characteristics of lightweight concrete slab–column connections falling in punching shear. ACI Struct J 1993;90(4):342–55.
[8] Cox BN, Marshall DB. Concepts for bridged cracks in fracture and fatigue. Acta Metall J 1994;42(2):341–63.
[9] Bentur A, Mindess S. Fiber reinforced cementitious composites. NY: Elsevier Applied Science; 1990. 620 pp.
[10] Beaudoin JJ. Handbook of fiber-reinforced concrete, principles, properties, developments and applications. Noyes Publications; 1990. 332 pp.
[11] Harajli MH, Maalouf D, Khatib H. Effect of fibers on the punching shear strength of slab–column connections. Cem Concr Compos 1995;17:161–70.
[12] ACI Committee 318. Building code requirements for structural concrete (ACI 318-02), vol. 87 (3). 1990. p. 350–61.
[13] Elgabry AA, Ghali A. Design of stud-shear reinforcement for slabs. ACI Strcut J 1990;87(3):350–61.
[14] Li V, Ward R, Hamza AM. Steel and synthetic fibers as shear reinforcement. ACI Mater J 1992;89(5):499–508.
[15] Parra-Montesinos GJ, Wight JK. Seismic response of exterior RC column-to-steel beam connections. J Struct Eng 2000;126(10):1112–21.
[16] Megally S, Ghali A. Punching shear design of earthquake-resistant slab–column connections. ACI Struct J 2000;97(5):720–30.
[17] EC 2. Design of concrete structures, part I: general rules and rules for buildings. European Committee for Standardization Brussels; 1991.
[18] CEB-FIP MC 90. Design of concrete structures. CEB-FIP-Model-Code 1990. Thomas Telford; 1993.
[19] BS 8110. Structural use of concrete, part 1, code of practice for design and construction. British Standards Institution; 1997.
[20] Khuntia M, Stojadinovic B, Goel SC. Shear strength of normal and high-strength fiber reinforced concrete beams without stirrups. ACI Struct J 1999;96(2):282–9.
[21] Naaman AE, Reinhardt HW. High performance fiber reinforced cement composites: HPFRCC 4. In: RILEM proceedings Pro 30. RILEM Publications SARL; 2003.
[22] Fanella DA, Naaman AE. Stress–strain properties of fiber reinforced mortar in compression. ACI J 1985;82(3):475–82.
[23] Oluokun FA. Prediction of concrete tensile strength from compressive strength: evaluation of existing relations for normal weight concrete. ACI Mater J 1991;88(3):302–9.
[24] Reda Taha MM, Shrive NG. Enhancing fracture toughness of high performance carbon fibre cement composites. ACI Mater J 2001;98(2):168–78.
[25] Naaman AE, Najm H. Bond-slip mechanisms of steel fibers in concrete. ACI Mater J 1991;88(2):135–45.
[26] Kotsovos MD, Pavlović MN. Ultimate limit-sate design of concrete structures: a new approach. London: Thomas Telford; 1998. 208 pp.
[27] Farhey DN, Adin MA, Yankelevsky DZ. Flat slab–column subassemblages under lateral loading. J Struct Eng 1993;119(6):1903–16.
[28] Reinhartd HW, Walraven JC. Crack in concrete subject to shear. J Struct Div 1982;108(ST1):207–24.
[29] Jelić I, Pavlović MN, Kotsovos MD. A study of dowel action in reinforced concrete beams. Mag Concr Res 1999(April).
[30] Zararis PD, Papadakis GC. Diagonal shear failure and size effect in RC beams without web reinforcement. J Struct Eng 2001;127(7):733–42.
[31] Kinnunen S, Nylander H. Punching of concrete slabs without shear reinforcement. Transactions no. 158. Royal Institute of Technology, Stockholm; 1960. p. 112.
[32] Zaghool ERF, Rawdon de Paiva HA. Strength analysis of corner column–slab connections. J Struct Div 1973;99(ST1):53–70.
[33] Theodorakopoulos DD, Swamy RN. Ultimate punching shear strength analysis of slab–column connections. Cem Concr Compos 2002;24:509–21.
[34] Regan PE, Braestrup MW. Punching shear in reinforced concrete—a state-of-art report by CEB Bull. 168, Lausanne, January 1985. p. 232.
[35] Chen WF. Plasticity in reinforced concrete. New York: McGraw-Hill; 1982. p. 204–5.

[36] Kupfer HB, Hildorf HK, Rusch H. Behavior of concrete under biaxial stresses. ACI J 1969;66(8):656–66.
[37] Naaman AE, Reinhardt HW. High performance fiber reinforced cement composites: HPFRCC 2. RILEM, E&FN SPON; 1996. p. 291–347.
[38] Fraser DJ. Elastic analysis of laterally loaded frames. J Struct Eng 1983;109(6):1479–89.
[39] Bažant ZP, Cao Z. Size effect in punching shear failure of slabs. ACI Struct J 1987;84(1):44–53.
[40] Marzouk H, Osman M, Hussein A. Punching shear of slabs: crack size and size effects. Mag Concr Res 2002;54(1):13–21.
[41] Alexander SDB, Simmonds SH. Punching shear tests of concrete slab–column joints containing fiber reinforcement. ACI Struct J 1992;89(4):425–32.
[42] McHarg PJ, Cook WD, Mitchell D, Yoon Young-Soo. Benefits of concentrated slab reinforcement and steel fibers on performance of slab–column connections. ACI Struct J 2000;97(2):225–34.